Published in final edited form as:
Mol Cancer Res. 2011 July ; 9(7): 901–913. doi:10.1158/1541-7786.MCR-10-0345.

Telomere dysfunction promotes metastasis in a Terc null mouse model of head and neck cancer

Bojana Bojovic and **David L. Crowe***
University of Illinois Cancer Center, University of Illinois at Chicago, 801 S. Paulina St., Room 530C, MC860, Chicago, IL 60612 tel: 312-996-9488 fax: 312-413-1604

Abstract

Squamous cell carcinoma arises from highly proliferative basal layer epithelial cells which normally divide for a short time before detaching from the basement membrane and undergoing terminal differentiation. Basal layer cells in stratified epithelia express the reverse transcriptase known as telomerase. Most human cells do not express telomerase and therefore are subject to loss of telomeric DNA with age due to the inability of lagging strand synthesis to completely replicate chromosomal ends. Late generation telomerase deficient mice exhibit signs of premature aging including reduced function of proliferating cellular compartments. We examined development of squamous cell carcinoma in a telomerase deficient murine background with long and short telomeres. G1 Terc−/− mice (long telomeres) had fewer lymph node metastases which correlated with increased numbers of apoptotic cells in these tumors compared to wild type mice. However, G5 Terc−/− mice with short telomeres had increased metastatic tumor burden similar to wild type mice. This increased metastasis correlated with genomic instability and aneuploidy in tumor cells from G5 Terc−/− mice. A number of similarities with human SCC were noted in the mouse model, and dramatic differences in global gene expression profiles were demonstrated between primary and metastatic tumors. We concluded that telomere shortening promotes metastatic tumor development in a Terc null mouse model of head and neck cancer.

Keywords

DNA replication; mitotic clock; invasion; genomic instability; squamous cell carcinoma

INTRODUCTION

Squamous cell carcinoma of the head and neck (HNSCC) is the sixth most frequent cancer worldwide (1). HNSCC is a major cause of morbidity and mortality in developing nations, comprising up to 50% of all malignancies. HNSCC is the most common malignant tumor of the oral cavity with 35,000 new cases and 8,000 deaths reported in the United States each year (2). Tobacco carcinogens are the primary etiologic agents of the disease, with age and genetic background as contributory factors. The overall 5 year survival rate of ~50% has not changed significantly in recent decades.

HNSCC arises from stratified squamous epithelium which is composed of multiple cell layers at distinct stages of differentiation with markedly different capacities for proliferation (3, 4). The highly proliferative basal layer epithelial cells divide for a short time before detaching from the basement membrane, ceasing cell division, and undergoing terminal differentiation which is associated with specific molecular, cellular, and histologic changes.

*Corresponding author: dlcrowe@uic.edu.

Basal layer cells in stratified epithelia such as epidermis and mucosa express the reverse transcriptase known as telomerase (5, 6). Telomerase is a ribonucleoprotein which uses an RNA template to synthesize new DNA at chromosomal ends (telomeres). Most human cells do not express telomerase and therefore are subject to loss of telomeric DNA with age due to the inability of lagging strand synthesis to completely replicate chromosomal ends. Loss of telomeric DNA can result in unprotected critically short telomeres, DNA damage response in the form of non-homologous end joining, cell cycle arrest, and apoptosis (7, 8). Late generation telomerase deficient mice exhibit signs of premature aging including reduced function of proliferating cellular compartments. Short telomeres in telomerase deficient mice can result in non-reciprocal translocations leading to genomic instability and increased cancer risk when tumor suppressor function is compromised (9–11). Telomerase is sufficient to immortalize human fibroblasts, and the vast majority of human cancers overexpress this enzyme which has been associated with poor clinical prognosis (12–14).

Telomere length has been shown to predict age related pathologies in humans including cancer (for review see 15). In human oral epithelium, telomere length has been shown to decrease with age (16, 17). In a series of cancer patients, 59% of individuals with HNSCC were in the shortest quartile for telomere length measured in peripheral blood lymphocytes (18). Telomere length also was significantly shorter in tumor cells compared to adjacent normal tissue (19). Telomerase expression was higher in HNSCC than in oral intraepithelial neoplasia and normal mucosa (20). High telomerase expression correlated with large tumor size, advanced clinical stage, higher recurrence rate, and lower survival rate in this study.

Our previous studies demonstrated that loss of telomerase expression during suprabasal differentiation of stratified epithelial cells was mediated by formation of a transcriptional repressor complex containing Rb and histone deacetylases at novel E2F sites in the telomerase promoter (21–23). Genetic mutations commonly found in epithelial cancers also play a role in maintaining telomerase expression in the suprabasal cells of stratified epithelium (24, 25). Thus the initial alteration in telomerase expression in dysplastic lesions of stratified epithelia is the failure to appropriately downregulate activity of the gene during suprabasal differentiation (26). These results raise interesting questions about the development of SCC in a telomerase deficient background and the effects of telomere length on the pathogenesis of this disease. In this study, we used our previously published chemical carcinogenesis protocol (27) which induces primary and metastatic HNSCC in 100% of animals to treat G1 Terc−/− mice with long telomeres and G5 Terc−/− animals with short telomeres. Our results indicate that decreased metastasis is the primary feature of HNSCC in G1 Terc−/− mice which correlates with increased apoptotic cells in these tumors. Critically short telomeres can compensate for loss of telomerase activity in metastasis of HNSCC arising in G5 Terc−/− mice due to increased genomic instability. HNSCC in Terc−/− mice showed genetic similarities with the human disease. Microarray analysis revealed that primary and metastatic HNSCC express markedly different gene expression profiles. We concluded that telomere shortening promotes metastasis during carcinogenesis.

MATERIALS AND METHODS

Transgenic Mouse Procedures

This study was approved by the institutional animal care and use committee before any experiments were performed. The Terc null mutant mouse strain B6.Cg $Terc^{tm1Rdp}$ was purchased from The Jackson Laboratory (Bar Harbor, ME). C57Bl6J mice were used as Terc+/+ control animals. Mice were housed in approved environmentally controlled facilities on 12 h light-dark cycles with unlimited access to food and water. Genotyping was performed according to The Jackson Laboratory protocol using extracted tail DNA as the PCR template. Terc−/− mice were bred for five generations to create G5 animals. Twenty

male and female 1 month old Terc+/+, G1 Terc−/−, G5 Terc−/− were dosed orally twice weekly using 25 μg dimethylbenzanthracene (DMBA) dissolved in 20 μl ethanol. The time course and number of tumors were recorded for each animal. Mice were euthanized when any institutional criterion for experimental neoplasia in rodents was met. Euthanized mice were photographed and complete necropsies were performed. A portion of each tumor specimen was flash frozen in liquid nitrogen or fixed in 4% buffered formaldehyde for 16 h at room temperature.

Histopathology and Immunohistochemistry

Tumor tissue was dehydrated in an ethanol series, cleared in xylene, and embedded in paraffin. Five micrometer sections were prepared and mounted on poly-L-lysine coated slides. Representative sections were stained with hematoxylin and eosin and histologically evaluated by a pathologist. Immunohistochemical analysis was performed using a commercially available kit (Invitrogen, Carlsbad, CA). Sections were incubated at 60° C for 30 minutes and deparaffinized in xylene. Endogenous peroxidase activity was quenched by incubation in a 9:1 methanol/30% hydrogen peroxide solution for 10 minutes at room temperature. Sections were rehydrated in PBS (pH 7.4) for 10 minutes at room temperature. Sections were blocked with 10% normal serum for 10 minutes at room temperature followed by incubation with anti-EGFR, cyclin A, cyclin B, cyclin D, cyclin E, c-myc, and PCNA antibodies (Santa Cruz Biotechnology, Santa Cruz, CA) for 16 hours at room temperature. After three washes in PBS, the sections were incubated with secondary antibody conjugated to biotin for 10 minutes at room temperature. After additional washes in PBS, the sections were incubated with streptavidin conjugated horseradish peroxidase for 10 minutes at room temperature. Following final washes in PBS, antigen-antibody complexes were detected by incubation with hydrogen peroxide substrate solution containing aminoethylcarbazole chromogen reagent. Slides were rinsed in distilled water, coverslipped using aqueous mounting medium, and allowed to dry at room temperature. The relative intensities of the completed immunohistochemical reactions were evaluated using light microscopy by independent trained observers who were unaware of the mouse genotypes. A scale of 0 to 3 was used to score relative intensity, with 0 corresponding to no detectable immunoreactivity and 1, 2, and 3 equivalent to low, moderate, and high expression respectively. Nonparametric data was analyzed by Fisher exact test.

Western Blot

Protein was extracted from microdissected primary and metastatic SCC in 1x Laemmli buffer. 50 μg total cellular protein was separated by SDS-PAGE on 10% resolving gels under denaturing and reducing conditions. Separated proteins were electroblotted to PVDF membranes according to manufacturer's recommendations (Roche Applied Science). Blots were incubated with antibodies to EGFR, cyclin A, cyclin B, cyclin D, cyclin E, c-myc, PCNA, p53, or β-actin for 16 hours at 4° C. After washing in Tris buffered saline containing 0.1% Tween 20 (TBST, pH 7.4), blots were incubated for 30 minutes at room temperature with anti-IgG secondary antibody conjugated to horseradish peroxidase. Following extensive washing in TBST, bands were visualized by the enhanced chemiluminescence method (Roche Applied Science). Bands were quantitated by densitometry.

Proliferation and Cell Death Analyses

Sterile BrdU solution (10 mg/ml in PBS; pH 7.4) was administered by intraperitoneal injection to tumor bearing Terc+/+, G1 Terc−/−, and G5 Terc−/− mice. Tumor tissue was fixed as described above, rehydrated in PBS, and incubated with either anti-BrdU antibody conjugated to fluorescein (proliferation analysis) or terminal deoxynucleotidyl transferase with dUTP-fluorescein (cell death) for 1 hour at 37° C (Roche Applied Science, Indianapolis, IN). After washing in PBS, proliferative or apoptotic cells were visualized by

fluorescence microscopy. The percentage of fluorescent cells in 10 random high power fields was determined.

Telomere Length Analysis

Average telomere length was measured by real time quantitative PCR from genomic DNA extracted from Terc+/+, G1 Terc−/−, and G5 Terc−/− microdissected normal mucosa and squamous cell carcinomas using established protocols (28). Forward and reverse telomeric primers were 5'- CGGTTTGTTTGGGTTTGGGTTTGGGTTTGGGTTTGGGTT −3' and 5'- GGCTTGCCTTACCCTTACCCTTACCCTTACCCTTACCCT −3'. The acidic ribosomal phosphoprotein PO (36B4) gene was used as the internal control. Forward and reverse primers for the 36B4 gene were 5'- ACTGGTCTAGGACCCGAGAAG −3' and 5'- TCAATGGTGCCTCTGGAGATT −3'. Each reaction contained PCR master mix (Bio-Rad), 300 nM each primer, and 20 ng genomic DNA. Reaction conditions for the telomere experiments were 95° C for 10 minutes followed by 30 cycles of data collection at 95° C for 15 sec and 56° anneal-extend for 60 sec. Reaction conditions for the 36B4 experiments were 95° C for 10 minutes followed by 35 cycles of data collection at 95° C for 15 sec, 52° annealing for 60 sec, and 72° C extension for 30 sec. Serial dilutions of mouse genomic DNA were amplified for standard curve calculation. Relative input amount of telomere PCR was divided by relative input amount of 36B4 PCR of the same sample. Real time PCR was performed a minimum of 3 times for each sample and the ratio of telomere:36B4 was calculated. The average of these ratios is the average telomere length ratio.

Comparative Genomic Hybridization Array Analysis

DNA was extracted from microdissected primary tumor tissue (n=3 for Terc+/+, G1 Terc−/−, and G5 Terc−/− groups) using a commercially available kit (Qiagen, Valencia, CA). For procedural quality control, analyses were performed as sex-mismatched hybridizations allowing chromosome X and Y copy number differences to be observed. One microgram of control and test genomic DNAs were fractionated, labeled with Cy3 or Cy5 dye, and hybridized to the mouse whole genome tiling set (385,000 probes/array, probe length 50–75 mer, median probe spacing 5782 bp; Nimblegen, Madison, WI). Signal intensity was combined with genome position data for each probe. Cy3 and Cy5 signal intensities were normalized to one another using qspline normalization. The data were then extracted for DNA segmentation analysis. This included a window averaging step using the Tukey biweight mean. A new position was assigned to this average which is the midpoint of the window. Adjacent windows were averaged which reduced noise within the data. The circular binary segmentation algorithm was used to segment the averaged log2 ratio data. DNA segments were called by attempting to break the segments into subsegments by looking at the t statistic of the means. One thousand permutations were performed to provide the reference distribution. If the resulting p value was below the threshold (p=0.01), a breakpoint was called. A pruning step was used to remove spurious segments, rejecting segments where the standard deviation of the means was not sufficiently different. A cutoff of 1.5 standard deviations was used.

Metaphase Spreads

Primary epithelial cell cultures derived from Terc+/+, G1 Terc−/−, and G5 Terc−/− tumors were treated with 0.1 μg/ml colcemid for 3 hours at 37° C. Cell pellets were suspended in 8 ml 60 mM KCl and incubated at room temperature for 30 minutes followed by prefixation with 2 ml 3:1 methanol:acetic acid. After centrifugation, cell pellets were fixed 3 times in methanol:acetic acid and spotted onto microscope slides. Cy3 labeled telomeric peptide-nucleic acid probe was hybridized to the metaphase spreads according to manufacturer's recommendations (Dako, Carpinteria, CA). After washing, slides were coverslipped using

Vectashield with DAPI (Vector Laboratories) and photographed using fluorescence microscopy.

RNA Extraction and Gene Expression Profiling

Total RNA was extracted from individual microdissected primary and metastatic G1 and G5 Terc−/− tumor tissue (n=3 for each group) using a commercially available kit (RNEasy, Qiagen, Valencia, CA). Individually matched well differentiated primary and metastatic tumor tissue was used in microarray analysis. Three independent samples from each group were used in gene expression analysis. The integrity of rRNA bands was confirmed by northern gel electrophoresis. Total RNA (10 μg) with spike in controls was reverse transcribed using a T7-oligo(dT) promoter primer in the first strand cDNA synthesis reaction. Following RNase H mediated second strand synthesis, the double stranded cDNA was purified and served as template in the subsequent in vitro transcription reaction. The in vitro transcription reaction was carried out in the presence of T7 RNA polymerase and a biotinylated nucleotide analogue/ribonucleotide mix for complementary RNA amplification and biotin labeling. The biotinylated complementary RNA targets were then purified, fragmented, and hybridized to Affymetrix GeneChip Expression arrays (Santa Clara, CA). The murine genome 430 2.0 microarray was used to interrogate 39,000 possible transcripts in each sample. After washing, hybridization signals were detected using streptavidin conjugated phycoerythrin. Affymetrix GCOS software was used to generate raw gene expression scores and normalized to the relative hybridization signal from each experiment. All gene expression scores were set to a minimum value of 2 times background determined by GCOS software in order to minimize noise associated with less robust measurements of rare transcripts. Normalized gene expression data was imported into dChip sotware for hierarchical clustering analysis using the average linkage algorithm. Raw data was analyzed for quality control and the significance of differential gene expression determined by t test ($p < 0.05$) and ratio analysis (>2 fold).

RESULTS

We characterized the phenotype of chemically induced HNSCC in wild type, G1 Terc−/−, and G5 Terc−/− mice. We first examined the gross and histopathologic appearance of wild type, G1 Terc−/−, and G5 Terc−/− tumors. As shown in Fig. 1A, primary HNSCC in wild type and Terc−/− mice which began the induction protocol at 1 month old grew to 1.5 cm within 12 weeks after initial appearance. Histopathologic analysis of primary HNSCC in wild type and Terc−/− mice demonstrated well differentiated SCC in 70% (46 of 66 tumors analyzed) and moderate differentiation in 30% of cases (Fig. 1B, C). Histopathologic analysis of metastatic HNSCC in these groups of mice revealed moderately differentiated SCC in 90% of cases (178 of 202 tumors analyzed) and 10% well differentiated tumors (Fig. 1D). We concluded that the gross and histopathologic appearance of tumors was similar in wild type and Terc−/− mice.

We detected cervical lymph node metastasis in all groups of mice (Table 1). G1 Terc−/− mice showed statistically fewer metastatic nodes than wild type animals. 49 of 120 nodes were positive in G1 Terc−/− mice compared to 82 of 120 nodes analyzed in Terc+/+ animals ($p<0.01$). However, no statistically significant differences in the number of metastatic lymph nodes were observed between wild type and G5 Terc−/− mice (71 positive nodes of 120 analyzed; $p<0.09$). These results indicate that loss of telomerase activity in primary HNSCC reduces numbers of metastatic cells. However, short telomeres promoted metastasis in HNSCC arising in G5 Terc−/− mice. We examined number, latency, and growth rates of tumors in Terc+/+, G1 Terc−/−, and G5 Terc−/− mice. Tumor latency was 22 weeks in Terc+/+ mice and slightly increased (23 weeks; $p<0.4$) in Terc−/− mice (Fig. 2). Tumors required 13 weeks to reach 1.5 cm in greatest dimension in Terc+/+ mice and 12

weeks in Terc−/− animals. The number of tumors per mouse was similar between groups (1.7 for Terc+/+ and 1.6 in Terc−/−; data not shown). We concluded that there were no significant differences between Terc groups in number of tumors, latency, or growth rate.

To determine how Terc deficiency resulted in decreased numbers of metastatic cells, we examined proliferation and apoptosis in primary and metastatic tumors from Terc+/+, G1 Terc−/−, and G5 Terc−/− mice. As shown in Fig. 3A, the percentage of apoptotic cells in Terc+/+ tumors averaged 1.1%. In contrast, the percentage of apoptotic cells in Terc−/− tumors was 5.5% ($p<0.04$). This increase in apoptotic cells correlated with decreased tumor metastasis in G1 Terc−/− mice. We did not observe significant changes in the numbers of BrdU positive cells between Terc+/+ and Terc−/− tumors (Fig. 3B). BrdU labeling was significantly less in metastatic tumors than primary cancers (1% vs. 10% respectively, $p < 0.03$). These results correlated with significantly reduced mean tumor volume in metastatic cancers (24 mm^3 vs. 220 mm^3 for primary tumors; $p<0.0002$). We concluded that reduced metastasis in Terc−/− tumors correlated with increased numbers of apoptotic cells, likely due to reduced telomere maintenance in the proliferating tumor cells.

We hypothesized that increased metastasis in G5 Terc−/− mice may be due to critically short telomeres giving rise to genomic instability and metastatic clones. To test this hypothesis, we compared average telomere length ratios in Terc+/+, G1 Terc−/−, and G5 Terc−/− normal mucosa and primary SCC (n=20 for each group). Compared to Terc+/+ tumors, average telomere length ratios were significantly lower in G1 Terc−/− and G5 Terc −/− cancers (0.78, 0.6, and 0.27 respectively; $p<0.02$). Average telomere length ratios were significantly lower in tumors compared to normal mucosa (2.1 vs. 0.78 for Terc+/+, 2.0 vs. 0.6 for G1 Terc−/−, and 1.22 vs. 0.27; $p<0.001$). We reasoned that this significant telomere shortening in G5 Terc−/− tumors might result in signal free ends, chromosomal fusions, and aneuploidy leading to increased numbers of metastatic clones. We compared metaphase spreads from Terc+/+, G1 Terc−/−, and G5 Terc−/− primary tumors. As shown in Fig. 5A, tumors from Terc+/+ mice exhibited low frequency of signal free ends (2.1%) and aneuploidy (modal chromosomal number 47 compared to normal mouse chromosomal number of 40; $p<0.03$). Robertsonian type fusions were rare in tumor cells from Terc+/+ mice. Tumor cells from G1 Terc−/− tumors higher frequency of signal free ends (6%) compared to Terc+/+ cells (Fig. 5B). The overall number of chromosomes was higher in G1 Terc−/− tumor cells compared to Terc+/+ cancers (modal chromosomal number 50; $p<0.02$). In contrast, cells from G5 Terc−/− tumors showed significantly increased signal free ends (15%; $p<0.05$), chromosomal fusions (7%; $p<0.003$), and a high degree of aneuploidy consistent with telomere dysfunction during tumorigenesis (Fig. 5C). G5 Terc−/− tumors exhibited the highest degree of aneuploidy (modal chromosome number 71; $p<0.001$). We concluded that increased genomic instability correlated with telomere dysfunction in G5 Terc−/− squamous cell carcinomas.

Given that short telomeres in G5 Terc−/− mice resulted in increased genomic instability leading to increased metastasis, we hypothesized that specific changes in gene copy number would be associated with this phenotype. We tested this hypothesis using comparative genomic hybridization as described in Materials and Methods. The statistically significant DNA copy number changes ($p < 0.01$) are shown in Table 2. Terc+/+ tumors showed gain of copy numbers in mouse chromosomal regions 1A, 9B, and 11A. Loss of copy number was observed on mouse chromosomal region 17D. In G1 Terc−/− tumors, gain of copy number was observed in mouse chromosomal regions 1A1, 11A, 11B, and 16B. In G5 Terc−/− tumors, gain of copy number was observed on mouse chromosomal regions 1A, 2H, 9B, 11A, 11B, and 16B. Loss of copy number was observed in mouse chromosomal regions 17D and 19C1–2 in G5 Terc−/− tumors. Gain of copy number on mouse chromosomal region 1A was observed in all tumors. Similar regions of DNA copy number changes were detected in

G1 and G5 Terc−/− tumors (11A, 11B, 16B). These results indicate that increased metastasis in G5 Terc−/− HNSCC correlates with specific DNA copy number changes in these tumors compared to Terc+/+ or G1 Terc−/− mice.

We hypothesized that the increased genomic instability observed in G5 Terc−/− tumors would result in increased gene expression changes resulting in metastasis. To test this hypothesis, we performed global gene expression profiling on G1 Terc−/− and G5 Terc−/− microdissected tumor cells using microarray analysis. We previously published global gene expression changes between primary and metastatic HNSCC in Terc+/+ mice (27). The most statistically significant gene expression changes are shown in Tables 3–5. As shown in Table 3, there were 275 differentially expressed genes between G1 and G5 Terc−/− primary tumors. These genes included differentiation related gene products (small proline rich protein 3, 12.8 fold), proteases (transmembrane protease, serine 11a, 4.2 fold), tumor suppressors (neurofibromatosis 1, −2.0 fold; retinoblastoma binding protein 4, −3.0 fold), and kinases (phosphatidylinositol 3-kinase, −3.5 fold). Comparison of metastatic tumors between G1 Terc−/− and G5 Terc−/− mice revealed 315 differentially expressed genes (Table 4). These genes included those regulating proteases (mannan binding lectin serine protease 2, 3.3 fold; tissue inhibitor of metalloproteinase 3, −2.9 fold), transcription factors (transcription factor 4, 2.9 fold; nuclear receptor subfamily 4, group A, member 2, 2.6 fold), kinases (glycogen synthase kinase 3 beta, 2.1 fold), and tumor suppressors (retinoblastoma binding protein 4, −2.4 fold). These results indicate that primary tumors in G1 Terc−/− and G5 Terc−/− mice are related, as are metastatic tumors in these animals.

We also examined differences between primary and metastatic SCC in G5 Terc−/− mice. As shown in Table 5, we identified 857 differentially expressed genes between primary and metastatic HNSCC in G5 Terc−/− mice. These changes included loss of gene expression regulating differentiation and adhesion (keratin complex 1, acidic, gene 14, −701.2 fold; keratin complex 2, basic, gene 6b, −691.1 fold; plakophilin 1, −335.3 fold; keratin complex 2, basic, gene 6a, −181.9 fold; small proline rich protein 3, −125.6 fold; keratin complex 2, basic, gene 5, −118.3 fold; integrin beta 4, −28.0 fold; desmoplakin, −18.0 fold; cadherin 1, −7.7 fold; integrin alpha 6, −5.2 fold; Notch gene homolog 3, −2.9 fold). Genes involved in signal transduction were upregulated in metastatic SCC (G protein coupled receptor 18, 37.5 fold; serine/threonine kinase 23, 23.5 fold; protein kinase C, beta 1, 12.5 fold; regulator of G protein signaling 14, 7.2 fold; regulator of G protein signaling 18, 6.9 fold; c-src tyrosine kinase, 4.3 fold; serine/threonine kinase 4, 3.1 fold; Janus kinase 1, 2.7 fold; regulator of G protein signaling 19, 2.6 fold). Genes involved in cellular migration and metastasis were upregulated in metastatic SCC (Ras related C3 botulinum substrate 2, 14.4 fold; coronin, actin binding protein 1A, 14.2 fold; cathepsin O, 9.0 fold; cathepsin Z, 3.0 fold). These results indicate that cells from metastatic HNSCC are less differentiated, have decreased cellular adhesion, and possess increased signaling and metastatic capabilities compared to primary tumors.

We also examined cell cycle regulatory protein expression in HNSCC from G1 and G5 Terc −/− mice by immunohistochemistry. Expression of these proteins in primary and metastatic tumors in G1 Terc−/− mice is shown in Fig. 6A, B. EGFR and cyclin E were each overexpressed in 53% (22/43) of primary tumors. Cyclin A and cyclin B were overexpressed in 80% (34/43) of primary tumors. c-myc was overexpressed in 40% (17 of 43) primary tumors. Of the 43 primary tumors analyzed, EGFR expression correlated with expression of downstream cell cycle regulatory proteins in a significant number of cancers (cyclin A, 37 tumors, $p<0.04$; cyclin B, 36 tumors, $p<0.04$; cyclin E, 39 tumors, $p<0.002$; c-myc, 36 tumors, $p<0.03$). In metastatic tumors in Terc−/− mice, cyclin B was overexpressed in 39% (47 of 120) of analyzed tumors. Cyclin D was overexpressed in 49% (59 of 120) of metastatic tumors in Terc−/− mice. PCNA labeling index varied widely between metastatic

tumors, ranging from 10%-70% of tumor cells. Of 120 metastatic tumors analyzed, cyclin B and D expression correlated with expression of the proliferation marker PCNA in a significant number of cancers (109 cases, $p<0.02$). The percentage of Terc−/− tumors overexpressing each of these cell cycle regulatory proteins was similar to that found in our previous studies on human and Terc+/+ mouse tumor tissue (26, 27). We also compared expression of these gene products in G1 Terc−/− primary and metastatic SCC by western blot. As shown in Fig. 6C, EGFR expression by western blot ranged from undetectable to more than 50 fold induction in primary SCC ($p < 0.0001$). Cyclin A expression was more than 40 fold induced between low and high level expressing tumors ($p < 0.002$). Cyclin E expression was more than 18 fold induced between low and high expressing SCC ($p < 0.005$). c-myc expression was 4 fold induced between low and high expressing tumors ($p < 0.01$). PCNA expression was 20 fold induced between low and high expressing SCC ($p < 0.03$). p53 levels varied by 12 fold between low and high expressing tumors ($p < 0.01$). In metastatic SCC, PCNA expression varied by 8 fold among low and high expressing tumors (Fig. 6D; $p < 0.04$). Cyclin B levels were 25 fold induced between low and high expressing metastatic SCC ($p < 0.01$). Cyclin D levels were more than 100 fold induced between low and high expressing tumors ($p < 0.0005$). p53 expression was not detected in metastatic SCC in G1 or G5 Terc−/− mice (Fig. 6D, E), in agreement with our previously published study (27). We concluded that the mouse Terc−/− HNSCC model recapitulated expression of specific cell cycle regulatory proteins observed in Terc+/+ tumors.

DISCUSSION

The basal layer of stratified epithelia expresses low levels of telomerase activity, and squamous cell carcinomas are believed to arise as the result of malignant transformation of these rapidly dividing cells (5, 6). During the process of stratified epithelial transformation, premalignant lesions express progressively higher levels of telomerase (29). In order to determine the effects of telomerase deficiency on development of HNSCC, we used our previously developed chemical carcinogenesis protocol in G1 (long telomeres) and G5 (short telomeres) Terc−/− mice. Previous studies using the DMBA/TPA mouse skin carcinogenesis protocol demonstrated that telomerase deficient mice were resistant to tumor formation (30). These results correlate with reduced metastasis in our DMBA induced Terc −/− HNSCC model. Conversely overexpression of telomerase in mouse skin resulted in tumor promotion using the DMBA/TPA protocol (31). An important difference in our study is the use of multiple DMBA doses which produces metastatic SCC in all mice compared to the DMBA/TPA protocol in which a low rate of malignant conversion is observed. Our results using oral mucosa as the target tissue showed no significant differences in primary tumor latency (other than slight increases in Terc−/− mice) or growth rates in wild type, G1 Terc−/−, or G5 Terc−/− mice. These results indicate that primary tumor formation in our model is independent of telomerase activity and telomere length. This may be due to the fact that low levels of telomerase activity in normal stratified epithelia of wild type mice during early tumorigenesis are insufficient to prevent the telomere erosion resulting from increased cell divisions. These shorter telomeres may result in the minimal differences in primary tumor latency and proliferation when compared to those in telomerase deficient animals.

A key finding of our study was decreased cervical lymph node metastasis in HNSCC arising in G1 Terc−/− mice. In agreement with these findings, metastasis has been associated with increased telomerase activity has been noted in tumors from different tissues, including human oral cancer (32–34). Telomere uncapping results in cellular senescence and programmed cell death, which may limit production of metastatic clones as shown in G1 Terc−/− tumors in our present study. High levels of telomerase activity may allow chromosomal end maintenance in these potential clones until sufficient genetic changes have

occurred to produce metastasis. In this regard, long telomeres have been associated with decreased survival in human HNSCC (19).

In contrast to the decreased metastasis observed in G1 Terc−/− HNSCC, tumors from G5 Terc−/− mice regain metastatic capability. G5 Terc−/− HNSCC demonstrated an increased percentage of telomeric signal free ends in metaphase chromosomal spreads compared to G1 Terc−/− or Terc+/+ cancers. This percentage was higher than observed in spontaneous tumors arising in Terc/p53 null mice, likely due to additional telomere shortening resulting from the chemical carcinogenesis protocol (9). We hypothesized that increased genomic instability during tumorigenesis as the result of critically short telomeres in G5 Terc−/− mice might more efficiently produce metastatic clones. To test this hypothesis, we performed DNA copy number analysis using comparative genomic hybridization on tumor cells from Terc+/+, G1 Terc−/−, and G5 Terc−/− mice. The increased DNA copy number changes observed in G5 Terc−/− metastatic tumors were statistically significant. These changes were associated with markedly increased chromosomal fusions and aneuploidy. A number of these DNA copy number changes correspond to those found in human HNSCC (35; 17D and 3p, 19C1–2 and 9p21, 16B and 3q). Higher resolution analysis of these copy number changes will reveal specific genes which are amplified or deleted in metastatic HNSCC.

Global gene expression profiling of primary and metastatic tumor cells revealed important new information about signaling pathways that regulate HNSCC. Retinoblastoma binding protein 4 was downregulated in Terc−/− primary and metastatic tumors. Retinoblastoma binding protein 4 has been shown to have tumor suppressor function (36). Similarly kallikrein related peptidases which may promote invasion were upregulated in Terc−/− metastatic tumors (37). Cathepsins which have been shown to increase tumor cell proliferation, invasion and metastasis were overexpressed in Terc−/− metastatic tumors (38). Receptor signaling pathways were also deregulated in Terc−/− mice. G protein coupled receptors are overexpressed in human cancers such as lung (39). The G protein coupled receptor GPR18 was dramatically overexpressed in Terc−/− metastatic HNSCC in our mouse model. Ephrin signaling was downregulated in metastatic Terc−/− HNSCC tumors, which has also been demonstrated in colorectal cancer (40). Notch signaling has been shown to suppress invasive tumor growth (41). In this regard, Notch 3 and Notch ligands Jagged 1 and 2 were downregulated in Terc−/− tumors and the Notch antagonist Numb was upregulated. JAK/STAT signaling was upregulated in our mouse HNSCC model, and also is enhanced in the human disease (42). Phosphatidylinositol-3-kinase subunits were upregulated in HNSCC in our mouse models, which are important survival factors for these tumors (43). In addition to striking downregulation of genes controlling differentiation and intercellular adhesion, the gene expression profile of HNSCC metastases in this model was notable for the large number of differentially regulated genes involved in cytoskeletal organization, cell migration, and invasion. Previous reports have shown that Rho family members are overexpressed in human cancer (44), and expression of Rac2 was increased in our mouse HNSCC model. The nonreceptor tyrosine kinase c-src (upregulated in Terc−/− metastatic HNSCC) is overexpressed in human HNSCC and regulates both proliferation and invasion by these cells (45). Members of the nuclear hormone receptor family such as peroxisome proliferator activated receptor γ were upregulated in Terc−/− metastatic HNSCC. PPARγ has been shown to regulate differentiation of epidermis (46); the complex PPARγ gene expression changes in our mouse models will be the subject of future investigation.

In summary, critically short telomeres promote metastasis in Terc−/− HNSCC. Future experiments will determine the types of DNA damage in tumor initiating cancer stem cells

that occur at early stages of tumor development in Terc−/− mice that account for the distinct phenotypic differences in HNSCC in these models.

Acknowledgments

We thank Dr. Timothy Triche, Betty Schaub, and Sitara Waidyaratne (Genomics Core Facility, Children's Hospital, Los Angeles, CA) for assistance with microarray analysis. This study was supported by National Institutes of Health grant DE14283 to DLC.

REFERENCES

1. Moore SR, Johnson NW, Pierce AM, et al. The epidemiology of mouth cancer: a review of global incidence. Oral Dis. 2000; 6:65–74. [PubMed: 10702782]
2. Goldberg HI, Lockwood SA, Wyatt SW, et al. Trends and differentials in mortality from cancers of the oral cavity and pharynx in the United States, 1973–1987. Cancer. 1994; 74:565–572. [PubMed: 8033034]
3. Taylor G, Lehrer MS, Jensen PJ, Sun TT, Lavker RM. Involvement of follicular stem cells in forming not only the follicle but also the epidermis. Cell. 2000; 102:451–461. [PubMed: 10966107]
4. Watt FM. Stem cell fate and patterning in mammalian epidermis. Curr Opin Genet Dev. 2001; 11:410–417. [PubMed: 11448627]
5. Harle-Bachor C, Boukamp P. Telomerase activity in the regenerative basal layer of the epidermis in human skin and in immortal and carcinoma derived keratinocytes. Proc Natl Acad Sci USA. 1996; 93:6476–6481. [PubMed: 8692840]
6. Blackburn EH. Telomere states and cell fates. Nature. 2000; 408:53–56. [PubMed: 11081503]
7. Lee HW, Blasco MA, Gottlieb GJ, Horner JW, Greider CW, DePinho RA. Essential role of mouse telomerase in highly proliferative organs. Nature. 1998; 392:569–574. [PubMed: 9560153]
8. Rudolph KL, Chang S, Lee HW, Blasco M, Gottlieb GJ, Greider CW, DePinho RA. Longevity, stress response, and cancer in aging telomerase deficient mice. Cell. 1999; 96:701–712. [PubMed: 10089885]
9. Artandi SE, Chang S, Lee SL, Alson S, Gottlieb GJ, Chin L, DePinho RA. Telomere dysfunction promotes non-reciprocal translocations and epithelial cancers in mice. Nature. 2000; 406:641–645. [PubMed: 10949306]
10. Maser RS, DePinho RA. Connecting chromosomes, crisis, and cancer. Science. 2002; 297:565–569. [PubMed: 12142527]
11. Blasco MA. Mice with bad ends: mouse models for the study of telomeres and telomerase in cancer and aging. EMBO J. 2005; 24:1095–1103. [PubMed: 15775986]
12. Kim NW, Piatyszek MA, Prowse KR, et al. Specific association of human telomerase activity with immortal cells and cancer. Science. 1994; 266:2011–2014. [PubMed: 7605428]
13. Bodnar AG, Ouellette M, Frolkis M, et al. Extension of lifespan by introduction of telomerase into normal human cells. Science. 1998; 279:349–352. [PubMed: 9454332]
14. Sebastian S, Grammatica L, Paradiso A. Telomeres, telomerase, and oral cancer. Int J Oncol. 2005; 27:1583–1596. [PubMed: 16273215]
15. Finkel T, Serrano M, Blasco MA. The common biology of cancer and aging. Nature. 2007; 448:767–774. [PubMed: 17700693]
16. Lindsey J, McGill NI, Lindsey LA, Green DK, Cooke HJ. In vivo loss of telomeric repeats with age in humans. Mut Res. 1991; 256:45–48. [PubMed: 1944386]
17. Nakamura K, Izumiyama-Shimomura N, Sawabe M, et al. Comparative analysis of telomere lengths and erosion with age in human epidermis and lingual epithelium. J Invest Derm. 2002; 119:1014–1019. [PubMed: 12445186]
18. Wu X, Amos CI, Zhu Y, et al. Telomere dysfunction: a potential cancer predisposition factor. J Natl Cancer Inst. 2003; 95:1184–1186. [PubMed: 12928335]
19. Patel MM, Parekh LJ, Jha FP, et al. Clinical usefulness of telomerase activation and telomere length in head and neck cancer. Head Neck. 2002; 24:1060–1070. [PubMed: 12454944]

20. Chen HH, Yu CH, Wang JT, et al. Expression of human telomerase reverse transcriptase (hTERT) protein is significantly associated with the progression, recurrence, and prognosis of oral squamous cell carcinoma in Taiwan. Oral Oncol. 2007; 43:122–129. [PubMed: 16798059]
21. Nguyen DC, Crowe DL. Intact functional domains of the retinoblastoma gene product are required for downregulation of telomerase activity. Biochim Biophys Acta. 1999; 1445:207–215. [PubMed: 10320773]
22. Crowe DL, Nguyen DC, Tsang KJ, Kyo S. E2F-1 inhibits transcription of the human telomerase reverse transcriptase gene. Nuc Acids Res. 2001; 29:2789–2794.
23. Crowe DL, Nguyen DC, Ohannessian A. Mechanism of telomerase repression during terminal differentiation of normal epithelial cells and squamous carcinoma lines. Int J Oncol. 2005; 27:847–854. [PubMed: 16077937]
24. Crowe DL, Nguyen DC. Rb and E2F-1 regulate telomerase activity in human cancer cells. Biochim Biophys Acta. 2001; 1518:1–6. [PubMed: 11267653]
25. Kumar SK, Zain RB, Ismail SM, Cheong SC. Human telomerase reverse transcriptase expression in oral carcinogenesis – a preliminary report. J Exp Clin Cancer Res. 2005; 24:639–646. [PubMed: 16471328]
26. Nguyen DC, Parsa B, Close A, Magnusson B, Crowe DL, Sinha UK. Overexpression of cell cycle regulatory proteins correlates with advanced tumor stage in head and neck squamous cell carcinomas. Int J Oncol. 2003; 22:1285–1290. [PubMed: 12738995]
27. Ku TKS, Nguyen DC, Karaman M, Gill P, Hacia JG, Crowe DL. Loss of p53 expression correlates with metastatic phenotype and transcriptional profile in a new mouse model of head and neck cancer. Mol Cancer Res. 2007; 5:351–362. [PubMed: 17426250]
28. Callicott RJ, Womack JE. Real time PCR assay for measurement of mouse telomeres. Comp Med. 2006; 56:17–22. [PubMed: 16521855]
29. Bednarek A, Budunova I, Slaga TJ, Aldaz CM. Increased telomerase activity in mouse skin premalignant progression. Cancer Res. 1995; 55:4566–4569. [PubMed: 7553630]
30. Gonzalez-Suarez E, Samper E, Flores JM, Blasco MA. Telomerase deficient mice with short telomeres are resistant to skin tumorigenesis. Nature Genet. 2000; 26:114–117. [PubMed: 10973262]
31. Cayuela ML, Flores JM, Blasco MA. The telomerase RNA component Terc is required for the tumor promoting effects of Tert overexpression. EMBO Reports. 2005; 6:268–274. [PubMed: 15731767]
32. Saito Y, Kosugi S, Suda T, et al. Telomerase activity and metastasis: expansion of cells having higher telomerase activity within culture lines and tumor tissues. Japan J Cancer Res. 1997; 88:732–737. [PubMed: 9330604]
33. Umehara N, Ozaki T, Sugihara S, et al. Influence of telomerase activity on bone and soft tissue tumors. J Cancer Res Clin Oncol. 2004; 130:411–416. [PubMed: 15160288]
34. Koscielny S, Eggeling F, Dahse R, Fiedler W. The influence of reactivation of telomerase in tumor tissue on the prognosis of squamous cell carcinomas in the head and neck. J Oral Pathol Med. 2004; 33:538–542. [PubMed: 15357674]
35. O'Regan EM, Toner ME, Smyth PC, et al. Distinct array comparative genomic hybridization profiles in oral squamous cell carcinoma occurring in young patients. Head Neck. 2006; 28:330–338. [PubMed: 16470878]
36. Kong L, Yu XP, Bai XH, et al. RbAp48 is a critical mediator controlling the transforming activity of human papillomavirus type 16 in cervical cancer. J Biol Chem. 2007; 282:26381–26391. [PubMed: 17616526]
37. Singh J, Naran A, Misso NL, Rigby PJ, Thompson PJ, Bhoola KD. Expression of kallikrein related peptidases (KRP/hK5, 7, 6, 8) in subtypes of human lung carcinoma. Int Immunopharmacol. 2008; 8:300–306. [PubMed: 18182244]
38. Ohri SS, Vashishta A, Proctor M, Fusek M, Vetvicka V. The propeptide of cathepsin D increases proliferation, invasion, and metastasis of breast cancer cells. Int J Oncol. 2008; 32:491–498. [PubMed: 18202773]
39. Gugger M, White R, Song S, et al. GPR87 is an overexpressed G protein coupled receptor in squamous cell carcinoma of the lung. Disease Markers. 2008; 24:41–50. [PubMed: 18057535]

40. Cortina C, Palomo-Ponce S, Iglesias M, et al. EphB-ephrin B interactions suppress colorectal cancer progression by compartmentalizing tumor cells. Nature Genet. 2007; 39:1376–1383. [PubMed: 17906625]

41. Stella MC, Trusolino L, Pennacchietti S, et al. Negative feedback regulation of met dependent invasive growth by Notch. Mol Cell Biol. 2005; 25:3982–3996. [PubMed: 15870272]

42. Leong PL, Xi S, Drenning SD, et al. Differential function of STAT5 isoforms in head and neck cancer growth control. Oncogene. 2002; 21:2846–2853. [PubMed: 11973644]

43. Tsang KJ, Crowe DL. The mitogen activated protein kinase pathway is required for proliferation but not invasion of human squamous cell carcinoma lines. Int J Oncol. 1999; 15:19–23.

44. Pan Y, Bi F, Liu N, et al. Expression of seven main Rho family members in gastric carcinoma. Biochem Biophys Res Commun. 2004; 315:686–691. [PubMed: 14975755]

45. Zhang Q, Thomas SM, Xi S, et al. SRC family kinases mediate epidermal growth factor receptor ligand cleavage, proliferation, and invasion of head and neck cancer cells. Cancer Res. 2004; 64:6166–6173. [PubMed: 15342401]

46. Sertznig P, Seifert M, Tilgen W, Reichrath J. Peroxisome proliferator activated receptors (PPARs) and the human skin: importance of PPARs in skin physiology and dermatologic diseases. Am J Clin Dermatol. 2008; 9:15–31. [PubMed: 18092840]

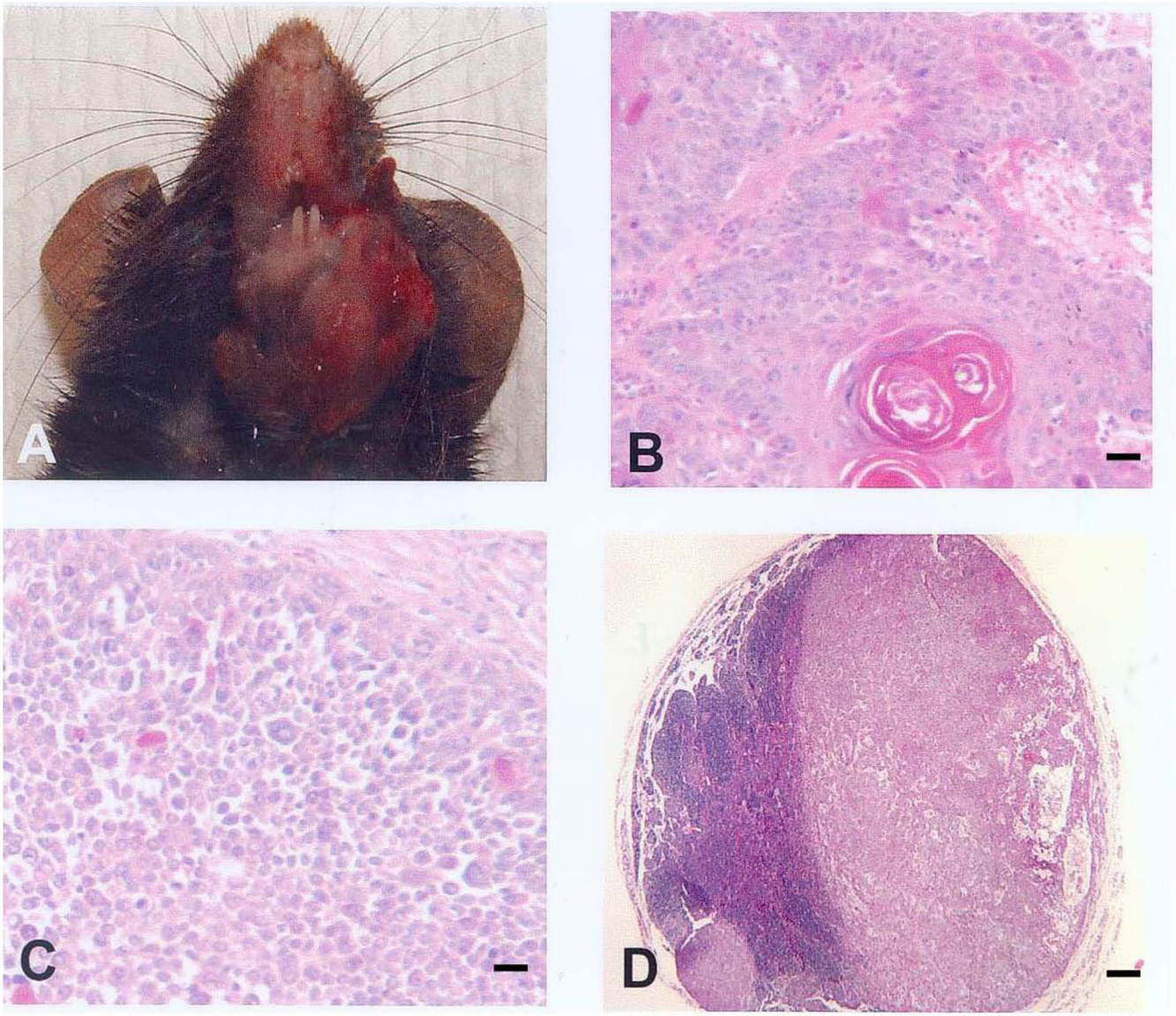

Fig. 1.

(A) Gross appearance of squamous cell carcinoma in vivo. (B) Hematoxylin and eosin stained section of well differentiated SCC in Terc−/− mice. Note well defined basal layer cells, multiple layers of differentiated suprabasal cells, and presence of keratin pearls. Magnification 100X. Scale bar = 50 μm. (C) Moderately differentiated SCC in Terc−/− mice. Epithelial differentiation is still apparent with a well defined basal layer but suprabasal differentiation is lacking. Magnification 100X. Scale bar = 50 μm. (D) Metastatic SCC in a cervical lymph node from Terc−/− mice. Moderately differentiated tumor cells occupy most of the lymph node in this section. Lymphocytes are seen on the left with a well demarcated boundary between these cells and the tumor. Magnification 20X. Scale bar = 200 μm.

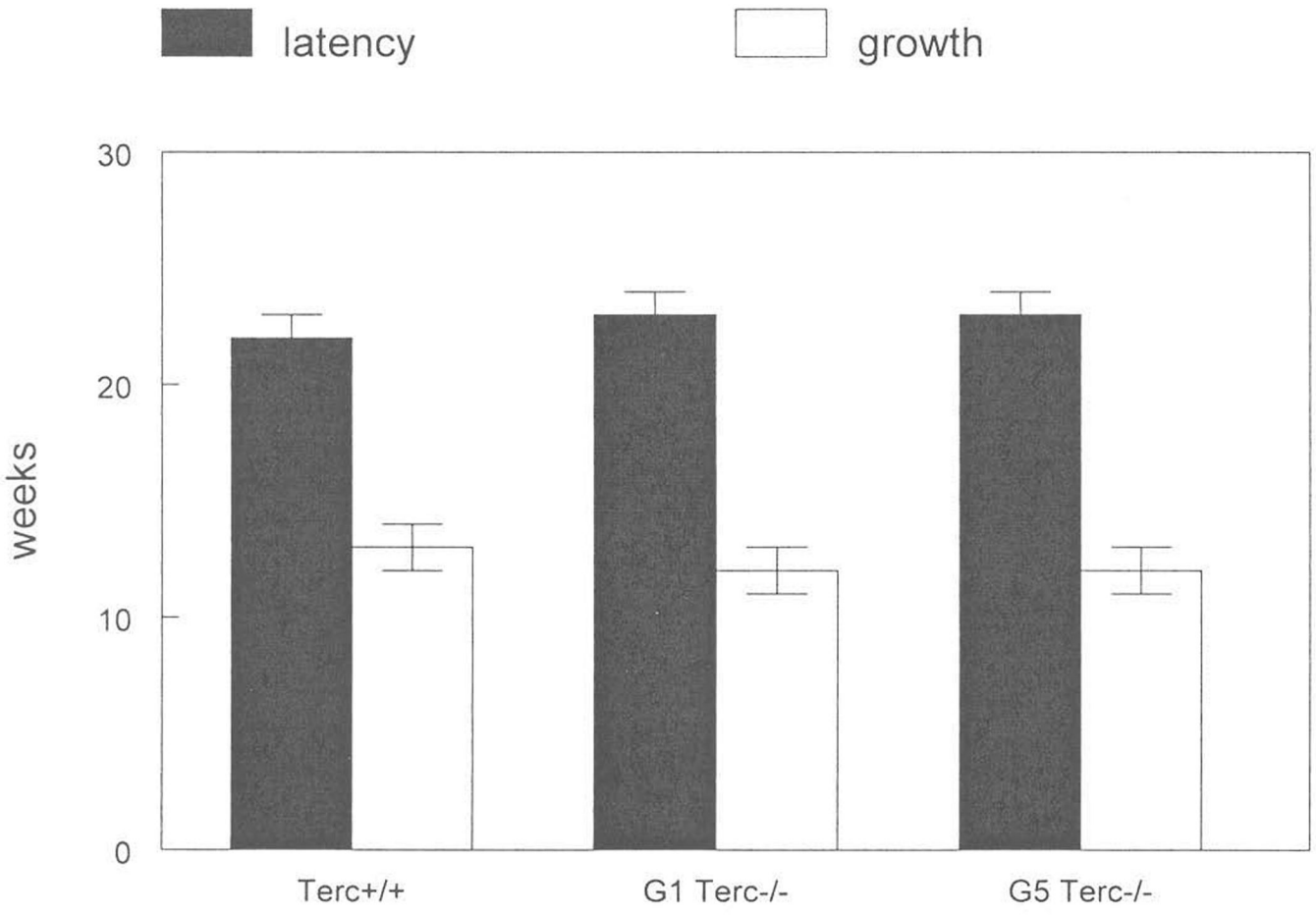

Fig. 2.

No differences in tumor latency or growth rates in Terc−/− mice. Animals were treated with the chemical carcinogenesis protocol described in Materials and Methods. The mean number of weeks to tumor development and time to achieve 1.5 cm in greatest dimension in Terc+/+, G1 Terc−/−, G5 Terc−/− mice is shown. Error bars indicate SEM.

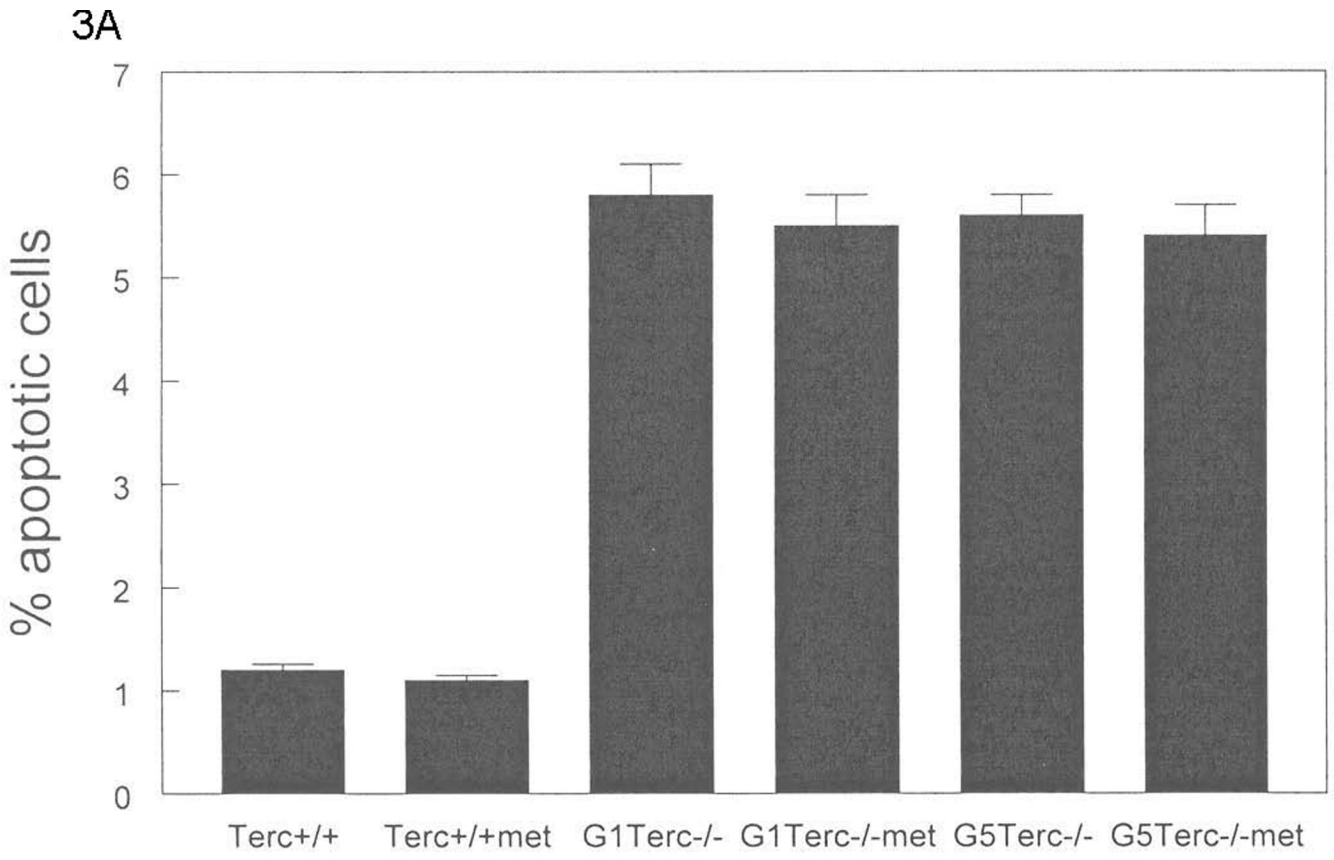

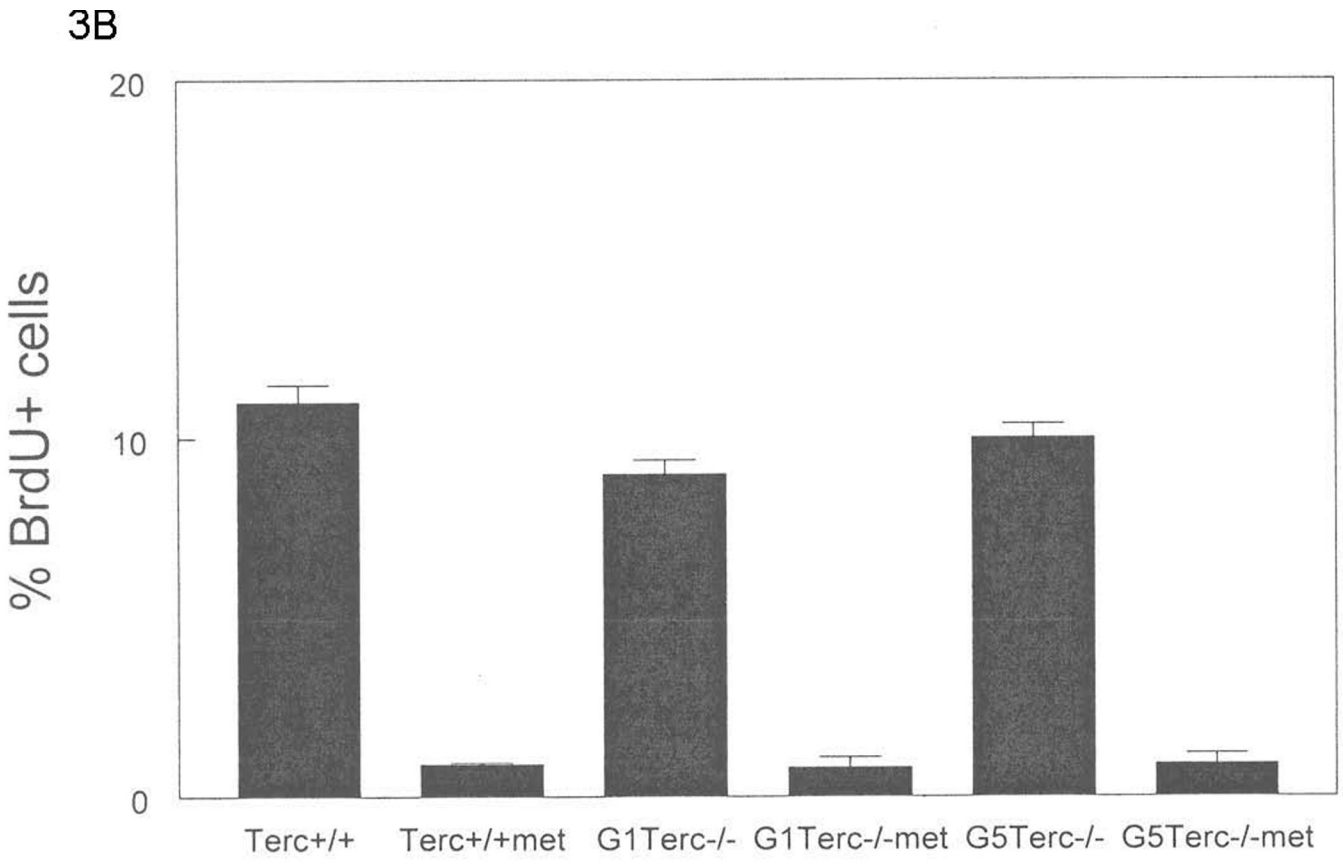

Fig. 3.

Increased apoptotic cells in primary and metastatic tumors from Terc−/− mice. (A) The number of apoptotic cells in tissue from primary and metastatic Terc+/+, G1 Terc−/−, and G5 Terc−/− tumors was analyzed as described in Materials and Methods. (B) No significant differences in proliferation rate of Terc+/+ and Terc−/− tumors. The number of BrdU positive cells in tissue from primary and metastatic Terc+/+, G1 Terc−/−, and G5 Terc−/− tumors was analyzed as described in Materials and Methods. Note proliferation of metastatic tumors was significantly decreased compared to primary cancers which correlated with significantly smaller volume of metastatic lesions. The percentage of fluorescent cells in 10 random high power fields was determined. Error bars indicate SEM.

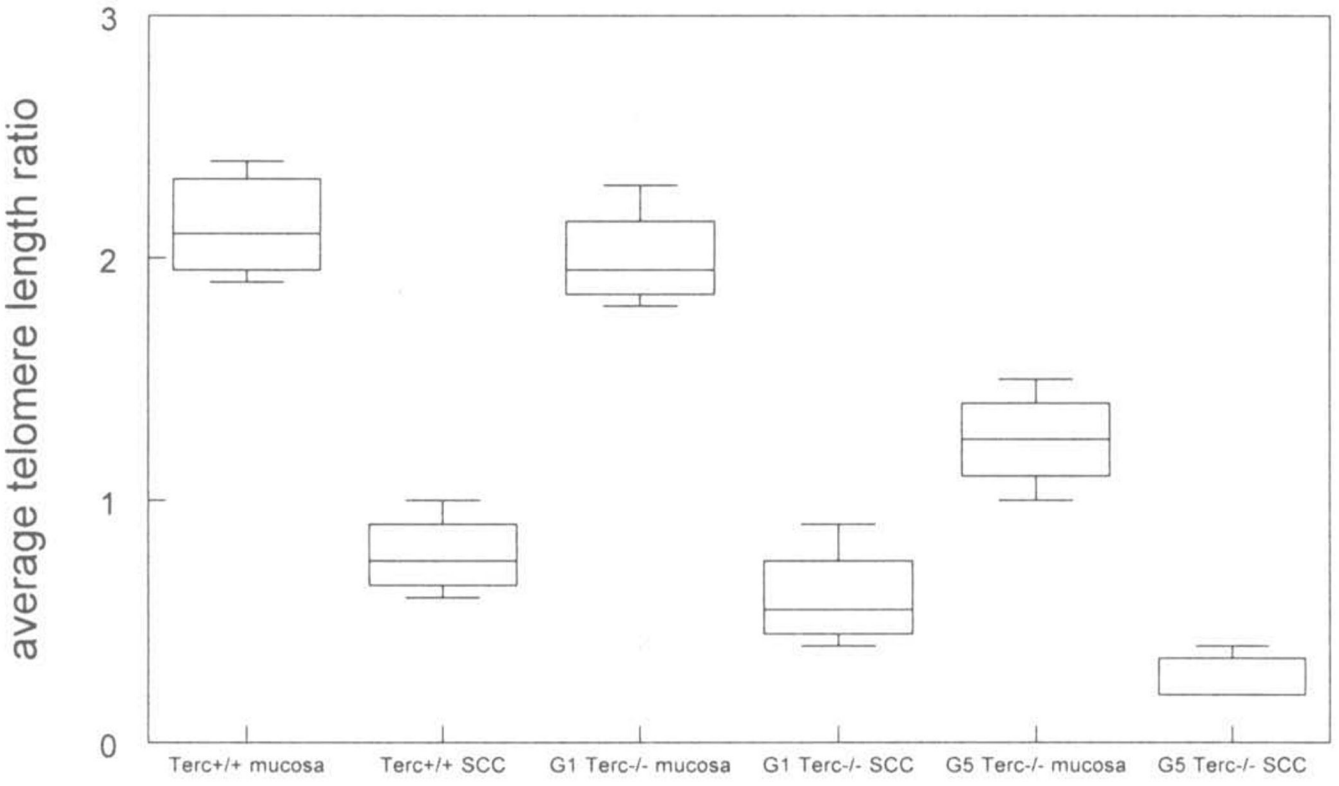

Fig. 4.

Terc deficiency correlates with shorter telomere length in squamous cell carcinomas. Average telomere length analysis of Terc+/+, G1 Terc−/−, and G5 Terc−/− normal mucosa and squamous cell carcinomas was performed as described in Materials and Methods. These experiments were performed three times with similar results.

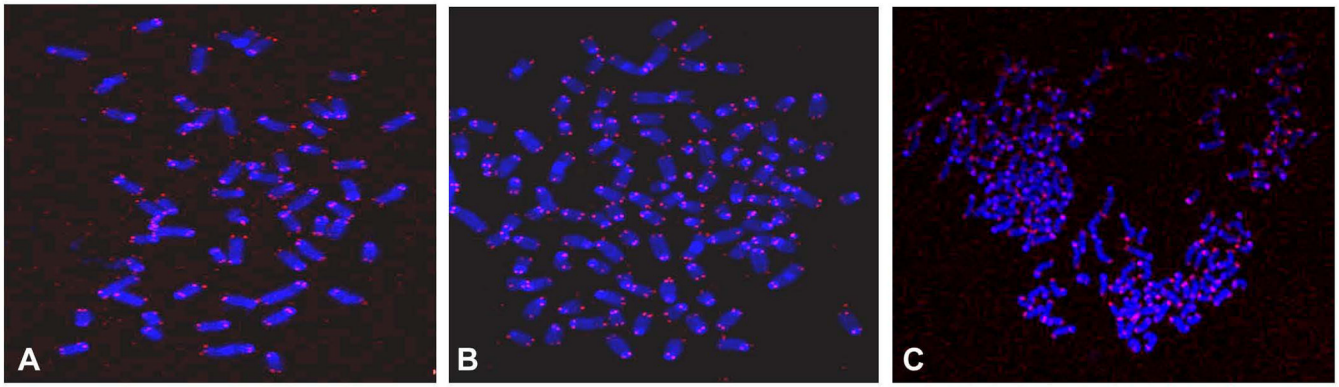

Fig. 5.

Compared to Terc+/+ (A) and G1 Terc−/− cancers (B), G5 Terc−/− tumors are characterized by chromosomal fusions and aneuploidy (C). Metaphase spreads and telomere fluorescence in situ hybridization were performed as described in Materials and Methods and photographed by fluorescence microscopy. Magnification 630X. These experiments were performed three times with similar results. Representative metaphase spreads are shown.

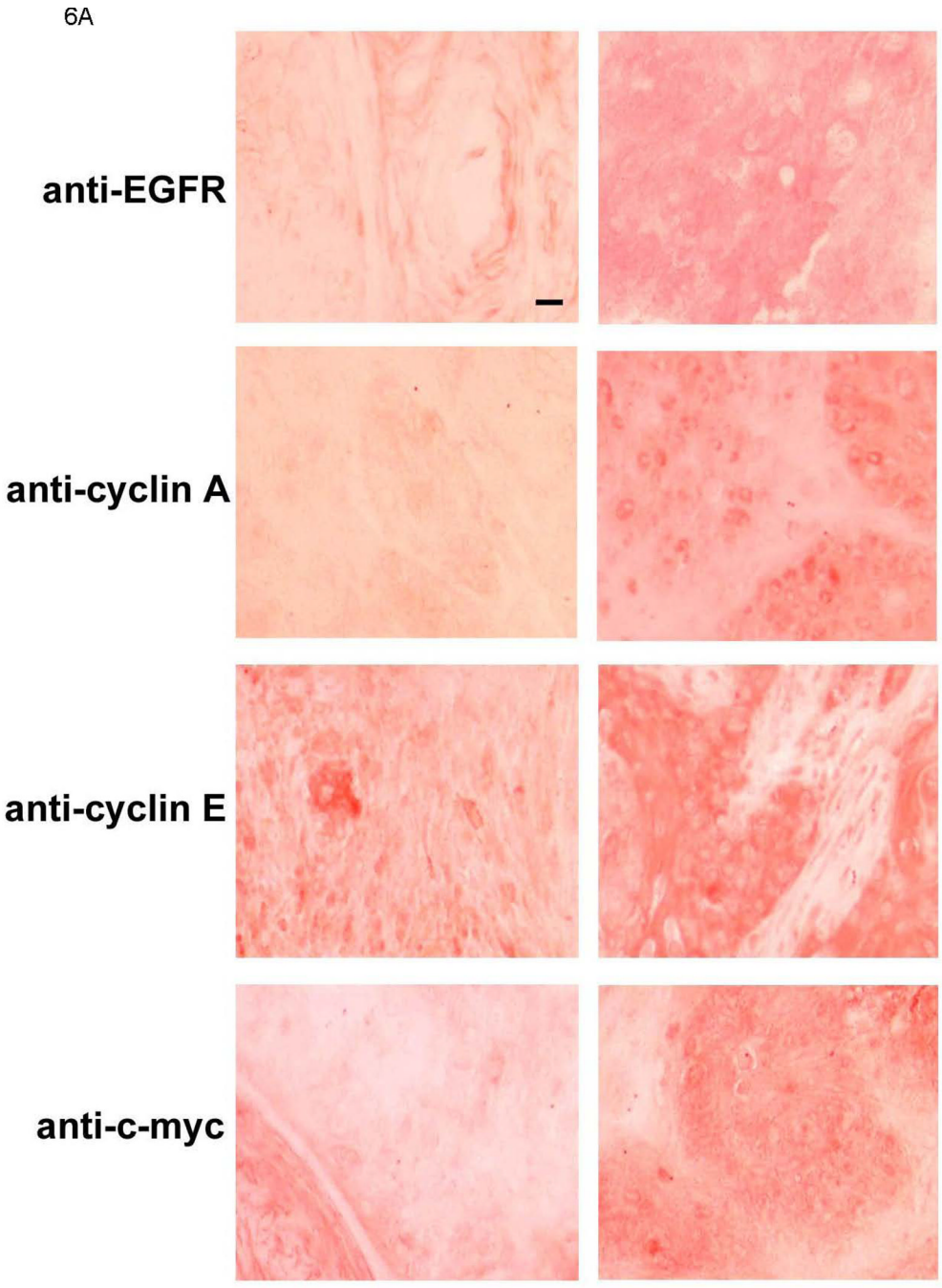

6B

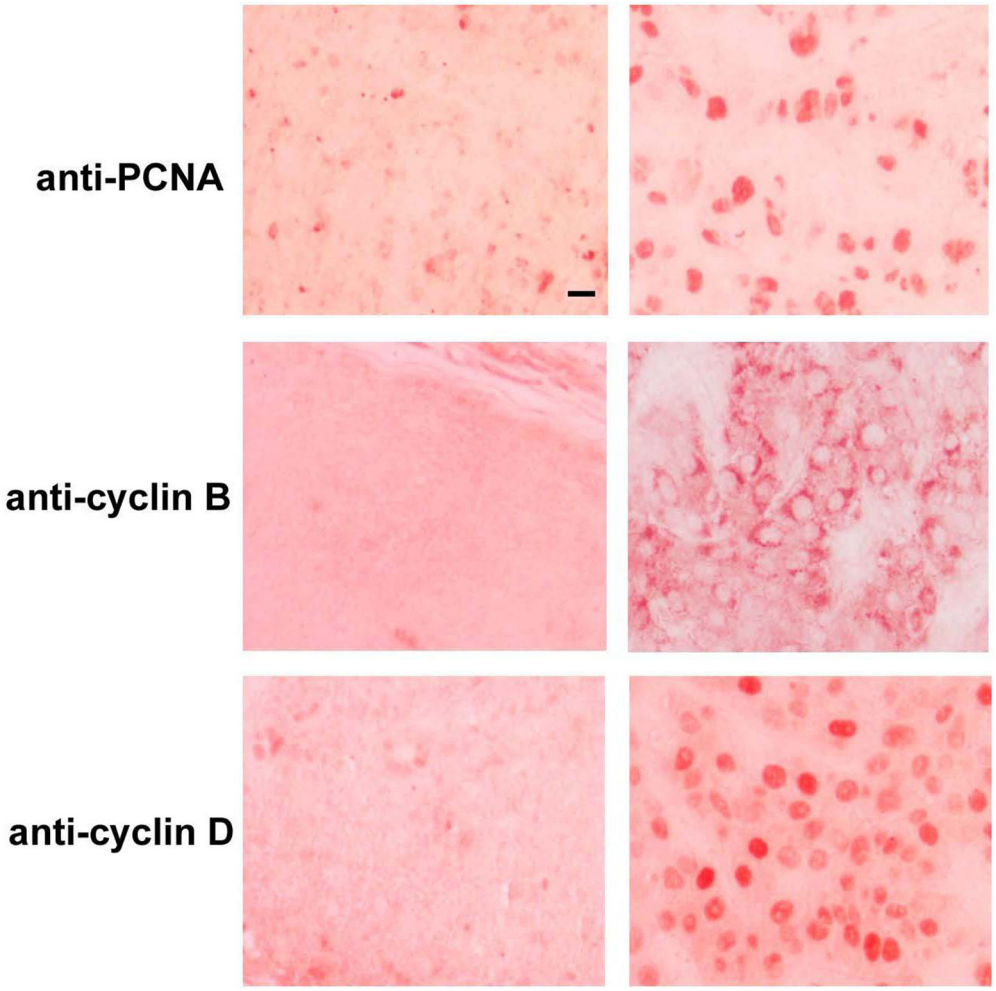

6C

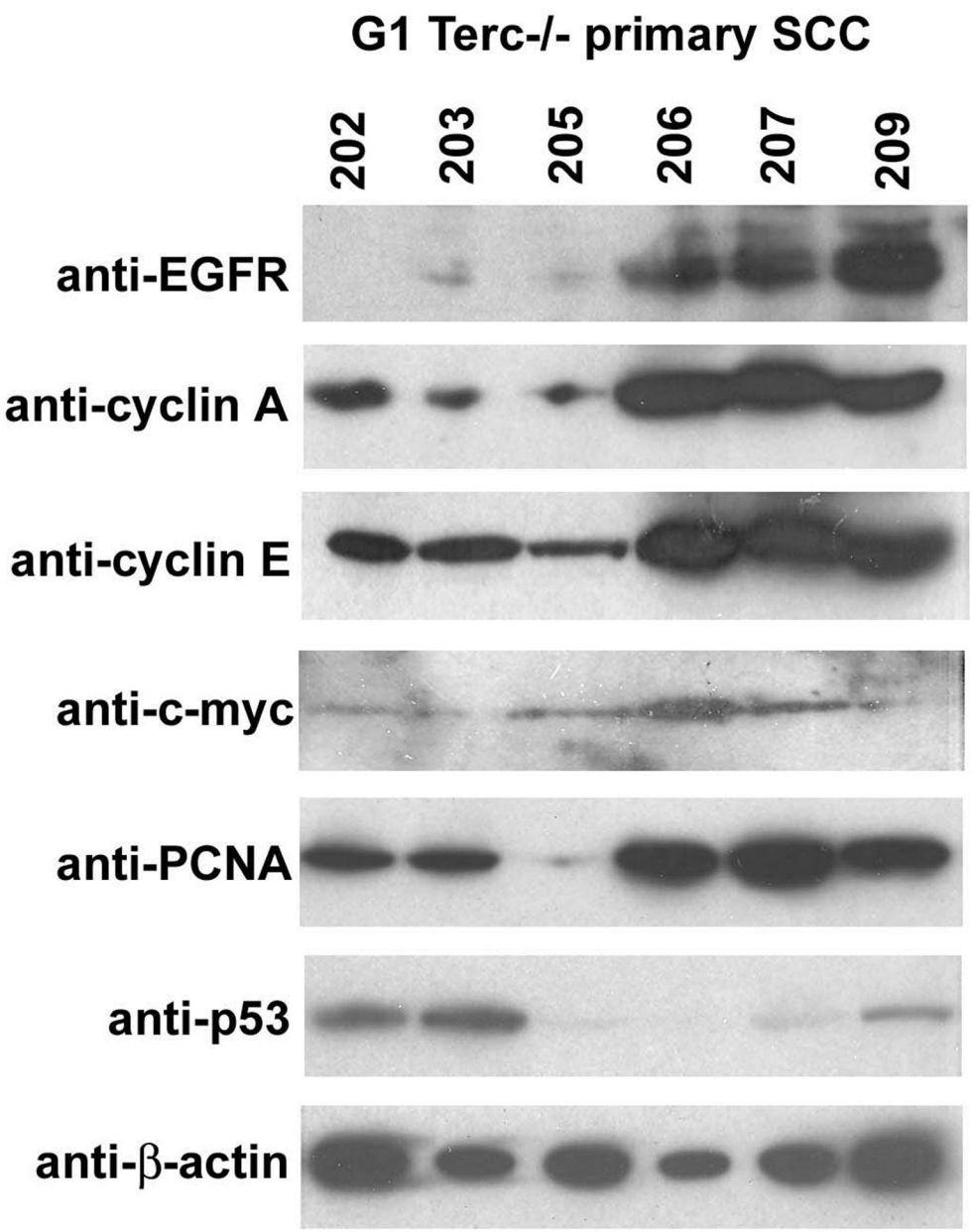

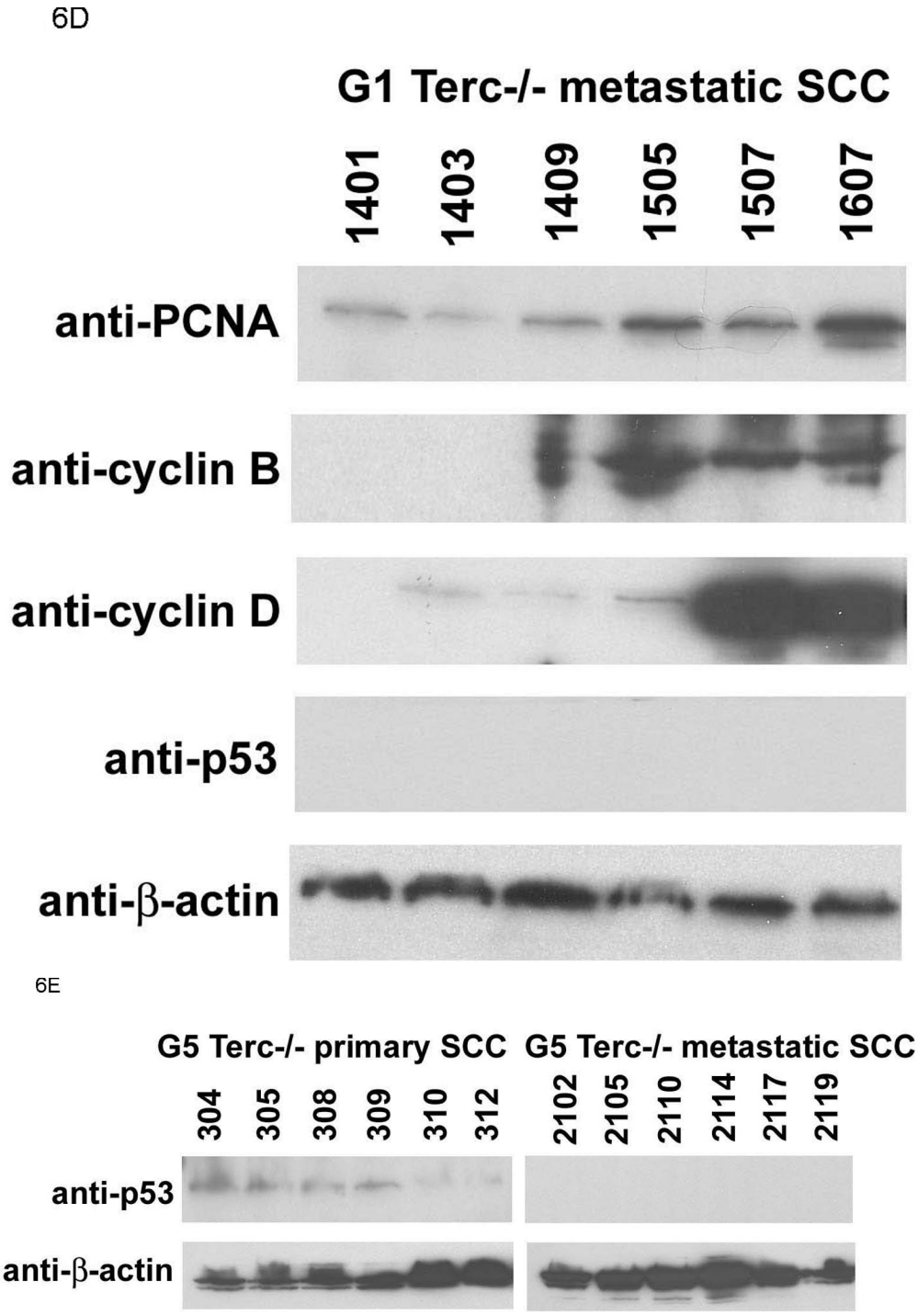

Fig. 6.

EGFR expression correlates with that of downstream cell cycle regulatory proteins in a significant number of primary SCCs in Terc−/− mice. (A) Immunohistochemistry was performed on G1 and G5 Terc−/− tumor sections using the indicated antibodies. Representative sections with low level expression are shown on the left and high level expression is shown on the right. (B) Cyclin expression correlates with proliferation index in a significant number of metastatic SCCs in G1 and G5 Terc−/− mice.

Immunohistochemistry was performed on tumor sections using the indicated antibodies. Representative sections with low level expression are shown on the left and high level expression is shown on the right. Magnification 400X. Scale bar = 10 μm. (C) Expression of cell cycle gene products (indicated at left) in primary G1 Terc−/− SCC is shown by western blot. Primary tumor identification numbers are shown at top of panel. These experiments were performed three times with similar results. Representative blots are shown. (D) Expression of cell cycle gene products (indicated at left) in G1 Terc−/− metastatic SCC is shown by western blot. Metastatic tumor identification numbers are shown at top of panel. (E) p53 expression in G5 Terc−/− primary and metastatic HNSCC is shown by western blot. Relative protein amount in each lane is shown by β-actin expression levels. These experiments were performed three times with similar results. Representative blots are shown.

Table 1

Percentage of metastatic lymph nodes in Terc+/+, G1 Terc−/−, and G5 Terc−/− HNSCC

	metastatic nodes	nodes analyzed/group	percent
Terc+/+	82	120	68.3
G1 Terc−/−	49	120	40.8
G5 Terc−/−	71	120	59.2

Table 2

Significant gene copy number changes in Terc+/+, G1 Terc−/−, and G5 Terc−/− primary SCC

Terc+/+ SCC		**G1 Terc−/− SCC**		**G5 Terc−/− SCC**	
Gain	**loss**	**gain**	**loss**	**gain**	**loss**
1A		1A1		1A	
				2H	
9B				9B	
11A		11A		11A	
		11B		11B	
		16B		16B	
	17D				17D
					19C1–2

Table 3

Gene expression changes between G1 Terc−/− and G5 Terc−/− primary SCC (278 genes)

Accession	Symbol	Gene name	fold change
NM_011478	Sprr3	small proline-rich protein 3	12.8
BB524685	Tmprss11a	transmembrane protease, serine 11a	4.2
AK013726	Zc3hav1	zinc finger CCCH type, antiviral 1	3.6
AK019924	Gcnt2	glucosaminyl (N-acetyl) transferase 2, I-branching enzyme	3.6
AF288377	Klra18	killer cell lectin-like receptor, subfamily A, member 18	2.9
BB766562	Abcb8	ATP-binding cassette, sub-family B (MDR/TAP), member 8	2.8
BC003867	Fnbp1	formin binding protein 1	2.7
BB131106	Garnl3	GTPase activating RANGAP domain-like 3	2.5
BB522674	Slc8a1	solute carrier family 8 (sodium/calcium exchanger), member 1	2.4
M94967	Ptgs2	prostaglandin-endoperoxide synthase 2	2.3
BB175029	Zc3hdc3	zinc finger CCCH type domain containing 3	2.3
BI793804	Sox9	SRY-box containing gene 9	2.2
M18775	Mapt	microtubule-associated protein tau	2.2
BC027279	Blvrb	biliverdin reductase B (flavin reductase, NADPH)	2.0
BE952183	Wasf3	WAS protein family, member 3	−2.0
BB485186	Nf1	neurofibromatosis 1	−2.0
AF217002	Tpcn1	two pore channel 1	−2.0
NM_016675	Cldn1	claudin 1	−2.1
BQ044016	Enah	enabled homolog (Drosophila)	−2.1
AB045132	Dhrs4	dehydrogenase/reductase (SDR family) member 4	−2.1
NM_030721	Acox3	acyl-Coenzyme A oxidase 3, pristanoyl	−2.1
AI447357	Phospho1	Phosphatase, orphan 1	−2.3
NM_025425	Rpl3l	ribosomal protein L3-like	−2.4
BB743796	Gtf3c1	general transcription factor III C 1	−2.4
AU040918	Rbbp4	retinoblastoma binding protein 4	−3.0
M60651	Pik3r1	phosphatidylinositol 3-kinase, regulatory subunit, (p85 alpha)	−3.5

Table 4

Gene expression changes between G1 Terc−/− and G5 Terc−/− metastatic SCC (315 genes)

Accession	Symbol	Gene name	fold change
BB322201	Arx	aristaless related homeobox gene (Drosophila)	5.1
BC010773	Car8	carbonic anhydrase 8	3.3
NM_010767	Masp2	mannan-binding lectin serine protease 2	3.3
AK014626	Kcnk16	potassium channel, subfamily K, member 16	3.3
BB467201	Tcf4	transcription factor 4	2.9
NM_011859	Osr1	odd-skipped related 1 (Drosophila)	2.8
AV225567	Ccbe1	collagen and calcium binding EGF domains 1	2.6
NM_013613	Nr4a2	nuclear receptor subfamily 4, group A, member 2	2.6
AF402613	Fgd4	FYVE, RhoGEF and PH domain containing 4	2.6
AK004253	Synpo2l	synaptopodin 2-like	2.6
BB370469	Map3k12	mitogen activated protein kinase kinase kinase 12	2.5
AK005789	Dncl2b	dynein, cytoplasmic, light chain 2B	2.4
BB486740	Hif3a	hypoxia inducible factor 3, alpha subunit	2.2
BQ173949	Gsk3b	glycogen synthase kinase 3 beta	2.1
NM_015823	Acvrinp1	activin receptor interacting protein 1	2.0
AK019497	Sympk	symplekin	−2.3
AU040918	Rbbp4	retinoblastoma binding protein 4	−2.4
BB756794	Prkag2	protein kinase, AMP-activated, gamma 2 non-catalytic subunit	−2.4
AF117613	Hebp1	heme binding protein 1	−2.7
BG073135	Timp3	Tissue inhibitor of metalloproteinase 3	−2.9
AV246339	Sdccag33l	Serologically defined colon cancer antigen 33 like	−3.2
BB357585	Slc1a3	solute carrier family 1, member 3	−3.5
BB477196	Zbtb3	zinc finger and BTB domain containing 3	−3.7
BF303544	Vapb	vesicle-associated membrane protein associated protein B & C	−4.0
AA617392	Max	Max protein	−4.2

Table 5

Gene expression changes between G5 Terc −/− primary and metastatic SCC (857 genes)

Accession	Symbol	Gene name	fold change
AV053098	Klk6 /// Klk5	kallikrein 6 /// kallikrein 5	63.8
NM_028075	Tnfrsf13c	tumor necrosis factor receptor superfamily, member 13c	38.9
BG145550	Gpr18	G protein-coupled receptor 18	37.5
BB036235	Stk23	serine/threonine kinase 23	23.5
BB250384	Vcam1	vascular cell adhesion molecule 1	15.3
NM_011335	Ccl21b	chemokine (C-C motif) ligand 21b (serine)	14.9
NM_009008	Rac2	RAS-related C3 botulinum substrate 2	14.4
BC002136	Coro1a	coronin, actin binding protein 1A	14.2
X59274	Prkcb1	protein kinase C, beta 1	12.5
AF396935	Emr4	EGF-like module containing hormone receptor-like sequence 4	11.6
BG064103	Traf1	Tnf receptor-associated factor 1	9.2
BB085450	Ctso	cathepsin O	9.0
AI573431	Il7r	interleukin 7 receptor	8.3
BM246535	Arhgap15	Rho GTPase activating protein 15	8.3
D11374	Sipa1	signal-induced proliferation associated gene 1	8.1
NM_009910	Cxcr3	chemokine (C-X-C motif) receptor 3	7.7
L20048	Il2rg	interleukin 2 receptor, gamma chain	7.5
AF316985	Tlr1	toll-like receptor 1	7.3
NM_016758	Rgs14	regulator of G-protein signaling 14	7.2
BC012254	Gstt1	glutathione S-transferase, theta 1	7.0
NM_008348	Il10ra	interleukin 10 receptor, alpha	6.9
BB139986	Rgs18	regulator of G-protein signaling 18	6.9
BC026894	Il16	interleukin 16	6.8
AK002516	Arhgdib	Rho, GDP dissociation inhibitor (GDI) beta	5.5
BI251808	Cyp1b1	cytochrome P450, family 1, subfamily b, polypeptide 1	5.3
BM244064	Tde1	tumor differentially expressed 1	5.2
NM_011146	Pparg	peroxisome proliferator activated receptor gamma	5.2
AK013741	Ppm1k	protein phosphatase 1K (PP2C domain containing)	4.5
BG094076	Csk	c-src tyrosine kinase	4.3
NM_021420	Stk4	serine/threonine kinase 4	3.1
AV329219	Erg	Avian erythroblastosis virus E-26 (v-ets) oncogene related	3.1
NM_022325	Ctsz	cathepsin Z	3.0
AV025980	Coro7	coronin 7	2.9
BC026773	Cklfsf7	Chemokine-like factor super family 7	2.7
BQ032637	Jak1	Janus kinase 1	2.7
AK004360	Ppp3cb	protein phosphatase 3, catalytic subunit, beta isoform	2.7
BB233670	Rgs19	regulator of G-protein signaling 19	2.6
BG067961	Map4k5	mitogen-activated protein kinase kinase kinase kinase 5	−2.8
NM_008716	Notch3	Notch gene homolog 3 (Drosophila)	−2.9

Accession	Symbol	Gene name	fold change
BC006797	Efnb1	ephrin B1	−3.2
NM_016912	Cdkl2	cyclin-dependent kinase-like 2 (CDC2-related kinase)	−3.3
BC027080	Erbb2	v-erb-b2 erythroblastic leukemia viral oncogene homolog 2	−3.6
AV149605	Blmh	bleomycin hydrolase	−3.8
BM245170	Fosl2	fos-like antigen 2	−4.0
BC016250	Cdc42ep1	CDC42 effector protein (Rho GTPase binding) 1	−4.6
BM935811	Itga6	integrin alpha 6	−5.2
AU042807	Cdh1	cadherin 1	−7.7
AA388313	Efna3	Ephrin A3	−9.6
AV264681	Jag2	Jagged 2	−11.5
AV297961	Dsp	desmoplakin	−18.0
L04678	Itgb4	integrin beta 4	−28.0
BC006780	Krt2–5	keratin complex 2, basic, gene 5	−118.3
NM_011478	Sprr3	small proline-rich protein 3	−125.6
NM_008476	Krt2–6a	keratin complex 2, basic, gene 6a	−181.9
NM_019645	Pkp1	plakophilin 1	−335.3
NM_010669	Krt2–6b	keratin complex 2, basic, gene 6b	−691.1
BC011074	Krt1–14	keratin complex 1, acidic, gene 14	−701.2